Generation of an Atomic Beam by Using Laser Ablation for Isotope Separation Purposes

Juliana Barranco de Matos[1], **Márcio de Lima Oliveira**[1], **Emmanuela Melo de Andrade Sternberg**[1], **Marcelo Geraldo Destro**[2], **Rudimar Riva**[2], **Nicolau André Silveira Rodrigues**[2]*

[1]Instituto Tecnológico de Aeronáutica – São José dos Campos/SP – Brazil
[2]Instituto de Estudos Avançados – São José dos Campos/SP – Brazil

Abstract: *Atomic vapor laser isotope separation has been studied at the Institute for Advanced Studies for nuclear purposes since 1982, and recently it has been questioned about its potentialities for the aerospace area. Many applications from nuclear propulsion to electricity generation and space navigation have been found, which justify the study of isotope separation for aerospace applications. One of the key process, and the first step for atomic vapor laser isotope separation, is the production of a neutral vapor jet. This paper discussed the potentiality of using laser ablation as a tool to generate neutral metal vapor jet for isotope separation purposes. The basis for the discussion is a set of experimental results obtained at the Institute for Advanced Studies. The experiments were described, the results were analyzed using basic theoretical treatment found in the literature, and it was concluded that laser ablation is a potential tool for the generation of a neutral vapor jet for atomic vapor laser isotope separation purposes.*

Keywords: *Laser ablation, Laser isotope separation, Neutral jet generation.*

INTRODUCTION

Both stable and radioactive isotopes have many important applications in the aerospace area. Nuclear propulsion, based in very compact and highly enriched ^{235}U demanding nuclear reactors, has been pointed as having great potential for deep space navigation (Bennet, 2006). Electricity generation in spacecrafts that travel far from the sun are in general based on radioisotope thermoelectric generator (Bennet, 2006; Flicker *et al.*, 1964). Inertial sensors (accelerometers and gyrometers) need special low losses waveguides and fibers, which can be produced by combining different Si isotopes (Kato and Lamont, 1977). Lithium niobate is an optical material broadly used in electro-optics devices and circuits used in inertial optical platforms: lithium niobate with low content of ^{6}Li is shown to be less sensitive to cosmic radiation and to have a longer operational life than the ordinary LiNb (Riley, 1999). Magnetic and magneto-optical sensors responsivity can be improved if isotope contents are considered (Itoh *et al.*, 1999; Kamada *et al.*, 2009).

Isotopes are separated in many different ways, depending on the specific isotope, the desired amount, the production process, and application. The most used isotope separation methods are those based on centrifuges (Beams and Haynes, 1936; Kholpanov *et al.*, 1997), gas diffusion (Naylor and Backer, 1955), electromagnetic methods (Martynenko, 2009), thermal diffusion (Furry *et al.*, 1939; Rutherford, 1986), aerodynamic method (Becker *et al.*, 1967), ion exchange and chemical separation (Calusaru and Murgulescu, 1976; Kim *et al.*, 2001), plasma centrifuge (Prasad and Krishnan, 1987; Del Bosco *et al.*, 1987), ion cyclotron resonance – ICR (Dolgolenko and Muromkin, 2009; Louvet, 1995), atomic vapor laser isotope separation – AVLIS (Schwab *et al.*, 1998; Paisner, 1988), and molecular LIS – MLIS (Schwab *et al.*, 1998; Jensen *et al.*, 1982).

The main differences between two distinct isotopes are mass, nuclear volume and nuclear spin. Most of the isotope separation processes are based on mass difference, however, the methods based on lasers, generally called LIS methods rely on the subtle difference on electromagnetic radiation absorption spectra (Mack and Arroe, 1956). The Institute for Advanced Studies (IEAv) has studied isotope separation, both in MLIS and AVLIS, mainly in uranium enrichment for nuclear fuel production (Schwab *et al.*, 1998).

The isotope separation based on AVLIS process follows three steps: production of a neutral atomic beam; selective photoionization of the desired isotope, and collection of the photoionized atoms.

The first step depends on the isotope to be separated: a simple resistive heating can cause evaporation in low-melting temperature materials, whereas, for high melting temperature materials, electron beam heating is generally used (Schiller *et al.*, 1983). However, there are refractory materials for which even electron beams cannot produce the desired vapor.

Short-laser pulses can remove a fraction of a target surface, generating a plume made of neutral atoms, ions, clusters, and droplets of liquified material (Amoruso *et al.*, 1999; Capitelli *et al.*, 2004; Noll, 2012). Such process is called laser ablation. Near the target surface, both atoms and ions are in excited states and tend to decay to the ground or metastable state as the plume expands (Kools *et al.*, 1992). As far as the neutral fraction can be separated from the rest of the plume, laser ablation could be used as a neutral jet source for AVLIS.

All the references mentioned in the last paragraph deal with the behavior of the plasma in the target vicinity. However, the interest for isotope separation is far from the target surface, where the plume is not collisional anymore and most of the ions and neutral atoms have decayed to the ground or metastable states.

This paper presents an experimental study in order to investigate the assumption that laser ablation can be used to prepare a neutral atomic jet for AVLIS purposes. Firstly, laser ablation is discussed in the thermal regime, and the relevant parameters are presented. The experiments are described and the results are analyzed using basic theoretical models found in the literature. It is concluded that, under our experimental conditions, laser ablation is indeed a potential method for neutral jet production for further isotope separation, at least when tiny amounts of material are desired.

LASER ABLATION

Laser ablation is the general designation for the material removal, from a solid or liquid surface, by short laser pulses. In this paper, only the so-called thermal laser ablation will be considered since it corresponds to the present experimental conditions (Amoruso *et al.*, 1999). If a laser pulse illuminates an area A of a solid target, a fraction a_A of the pulse will be absorbed. If the target is metallic or a strong absorber, the laser energy will be absorbed in a very thin layer with the thickness given by the optical penetration length. For instance,

for metals illuminated by light in the visible, the optical penetration length is typically much smaller than the radiation wavelength (Born and Wolf, 2002). It is reasonable to suppose that all the laser pulse energy is absorbed in the target surface and transmitted to the target volume through heat conduction. During the pulse duration τ, the heat penetrates the sample a depth given by the thermal diffusion length (Eq. 1):

$$L_D = \sqrt{4\kappa T}, \tag{1}$$

where,
κ: is the thermal diffusion coefficient.

Usually, in thermal ablation experimental conditions, the diameter of the illuminated area is much larger then L_D, and the heat conduction can be treated as a 'semi-infinite solid uniformly illuminated' problem and the target surface temperature, at the end of the laser pulse, will be as in Eq. 2 (Duley, 1976):

$$T(0) = T_0 + \frac{2a_A I_0}{K}\left(\frac{\kappa\tau}{\pi}\right)^{1/2}, \tag{2}$$

where,
T_0: is the target temperature before the laser pulse,
I_0: is the laser intensity (power/illuminated area), and
K: is the thermal conductivity.

The mass m_E removed from one single laser pulse can be estimated by using calorimetry and neglecting the solid-liquid phase transformation and the temperature dependence on the specific heat c_E as in Eq. 3:

$$m_E = \frac{a_A \varepsilon_p}{c_E \Delta T + L_V}, \tag{3}$$

where,
ε_p: is the pulse energy,
ΔT: is the temperature variation from the room until the boiling temperature, and
L_V: is the vaporization enthalpy.

EXPERIMENTS

Figure 1 presents the basic experimental setup: the laser beam is focused on the sample surface, forming a 45º angle by a 200 mm focal length positive quartz lens; the sample is fixed to a computer controlled *xy* table, and the sensor is placed in the plume path, at different distances from the sample.
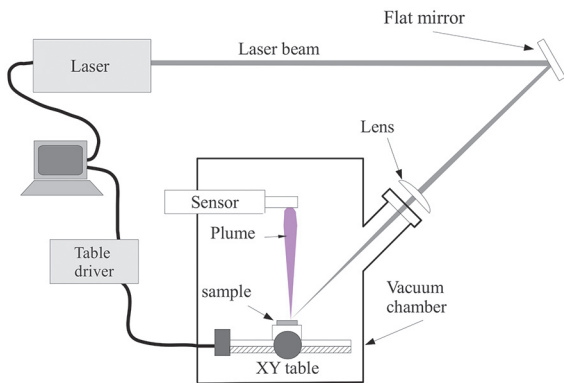
Figure 1. General experimental setup.

These experiments were performed in vacuum (~10^{-5} mbar), and three different sensors were used: a mass spectrometer, a piezoelectric polyvinylidene difluoride (PDVF) film, and an electrostatic probe. Three different lasers were used with the characteristics given in the Table 1.

A set of experiments of emission spectroscopy was accomplished in air. In such cases, a fraction of the light emitted by the plume was collected by a quartz lens, coupled to 500 um core optical fiber, delivered to an Ocean Optics spectrometer model HR4000 and later analyzed.

Mass spectrometry

In this set of experiments, the measuring device was a Pfeiffer quadrupole mass spectrometer model QMS-300, placed either at 10 or 25 cm from the target, with the ion collector placed orthogonally to the plume pathway. The lasers used in these experiments were the CuHBr and the CVL. Stainless steel, nickel, copper, tungsten, and tantalum targets were analyzed in two different measurements: the first with the

Table 1. Laser parameters

Parameter	CVL	CuHBr	Nd-YAG
Wavelength (nm)	511/578		355
Pulse width (ns)	40	35	25
Repetition rate (kHz)	5	16	2
Pulse energy (mJ)*	2.5	1	0.23
Peak power (kW)*	60	29	9.2
Average power (W)*	12.5	16	0.46
Illuminated area (cm²)	1.1×10^{-4}	1.5×10^{-5}	6.3×10^{-6}
Beam quality – M²	16.7	6	1.7
Peak power density (W/cm²)**	5.3×10^{8}	2.0×10^{9}	1.5×10^{9}
Fluency (J/cm²)	22	66	37

* maximum values; ** maximum value at target surface.

mass spectrometer ionization sector turned off and the second with the ionization sector turned on. With the ionization off, the ions captured by the mass spectrometer were only those produced in the laser ablation. With the ionization sector on, ions produced by impact of neutral atoms with electrons were added to those produced by laser ablation. For the stainless steel sample and the ionization sector turned off, peaks for Fe and Cr were observed, the main components of steel, and only singly ionized single atoms were present in the spectrograms, or rather, there were no peaks corresponding to ions doubly or highly ionized, not even for particles with the double of the unitary mass. For the ionization sector turned on, the spectra remained relatively the same, only the amplitude increased by a factor of about two. Although it is not possible to obtain quantitative information from this factor, because it is not clear which fraction of the neutral atoms are ionized in the ionization sector, it indicates that the ion and neutral populations have roughly the same order of magnitude. The same behavior was observed with all the remaining samples: only peaks due to single atoms singly ionized were observed. It is known that the plume generated by laser ablation is always followed by droplets; however, they were not seen in the mass spectrograms because the droplet mass was much above the mass spectrometer upper limit (300 amu). Thus, in our experimental conditions, except for the droplets, the monitored plume was mainly made of single atoms (neutral or singly ionized).

PVDF sensor

The PVDF is a polymer that exhibits pyro and piezoelectric properties, and PVDF films are suitable for time-of-flight (TOF) characterization in laser ablation experiments. It is very convenient to measure the plume drift velocity (center of mass velocity) and translational temperature both for neutral or ionized atoms. It is well-accepted that the plume generated by laser ablation of single element targets, far from the target surface, is mainly made of a bunch of atoms, which expand according to a maxwellian velocity distribution with a drift velocity; since the PVDF film responds to the plume as a pressure transducer, its TOF signal is given by Eq. 4 (Gião *et al.*, 2004):

$$S(t) \propto \frac{1}{t^5} \exp\left[-\frac{m}{2k_B T_Z}\left(\frac{l}{t} - v_0\right)^2\right]. \tag{4}$$

Considering the PVDF signal and fitting to Eq. 4, it is possible to obtain the drift velocity v_0 and the translational temperature T_z. These experiments were performed with a

HyBrID-copper laser and Fig. 2 provides a typical PVDF TOF signal, with the sensor placed 10 cm far from a tungsten sample; the solid lines indicate the PVDF signal and the dashed line represents the best fitting to Eq. 4. Table 2 gives some typical figures obtained during these experiments.
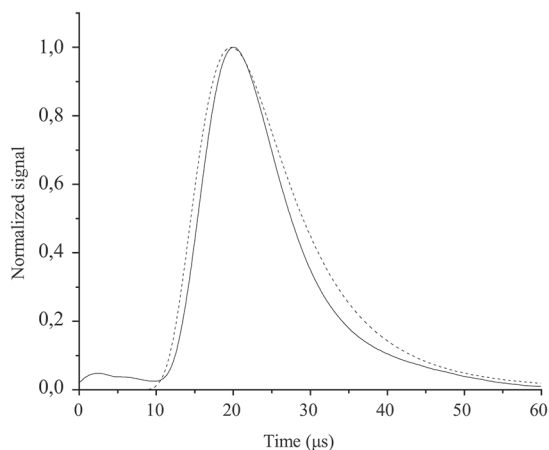

Figure 2. PVDF signal (solid line) and a best fit for Eq. 5 (dashed line) for ablation of tungsten with CuHBr laser.

Table 2. Plume parameters for ablation of tungsten targets measured with the PVDF sensor.

Target	Tungsten
Laser	CuHBr
Translational temperature (K)	$8.8 \times 10^4 - 9.1 \times 10^4$
Drift velocity (km/s)	$4.65 - 4.74$

Electrostatic probe

The electrostatic probe is convenient to measure drift velocity, translational temperature of ions, ion density, electron density and temperature (Chung, 1975). One electrostatic probe, made of a 10 mm long and 250 μm diameter tungsten wire, placed transversely to the plume, at distances ranging from 4 to 20 cm from the target, was used to study the plasma generated by ablation of tungsten targets. Firstly, the TOF signal of the ions was studied with the probe polarized at a -10 V voltage.

Later, the electrostatic probe was used to evaluate the charge densities and electron temperature. Figure 3 shows the probe current signal time behavior for different probe electric potentials in experiments with the CuHBr laser and W targets. The noise around 5×10^{-6} s is from laser electric discharge pulses, and it was taken as reference for triggering the oscilloscope. The peak values of the probe current curves were plotted against the polarization voltage, giving rise to the Langmuir curve. From this curve, the charge densities

and electron temperature were evaluated, considering the hydrodynamic expansion approach (Koopman, 1971). This experiment was repeated with aluminum and tungsten targets, ablated by CVL laser, and for copper samples, ablated by the Nd-YAG one. Typical results are shown in Table 3.
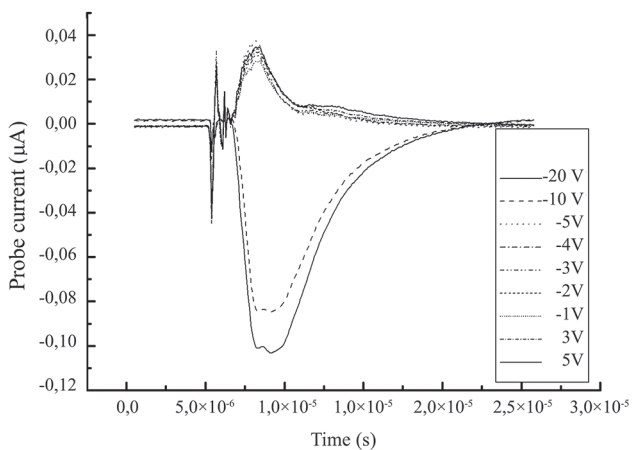

Figure 3. Temporal behavior of the probe current in different voltages, for ablation of tungsten samples with the CuHBr laser.

Table 3. Plasma parameters for ablation of different targets and lasers, measured with the electrostatic probe. All the listed figures are peak values.

Target	Copper	Aluminum	Tungsten	Tungsten
Laser	CVL	CVL	CuHBr	CVL
Ion density (m^{-3})	3.4×10^{16}	2.3×10^{15}	2.4×10^{17}	1.3×10^{16}
Electron density (m^{-3})	1.2×10^{15}	3.2×10^{14}	6.3×10^{15}	3.9×10^{14}
Electron temperature (eV)	15	19	28	15
Drift velocity (km/s)	$8 - 10$	$8 - 13$	5.4	$6 - 10$

Emission spectra

Laser induced breakdown spectroscopy (LIBS) experiments in air were made with copper, graphite, molybdenum, alumina, and beach sand samples in order to investigate the composition of the expanding plume. The plume light emission in our experimental conditions vanishes for distances larger than 3 or 4 mm and thus the experiments were performed just above the target surface and not at the same distances, as in the case of the PVDF and electrostatic probe experiments.

For the three first targets, since they were single element samples, the line attribution was made by comparing

the measured spectrum with a simplified synthetic one, considering only the sample constituent element. The synthetic spectrum was built by adding lorentzian curves with peak values given by the Einstein *A* coefficient, taken from the National Institute of Standards and Technology transitions database (NIST, 2012), and with the linewidth equals to the instrument resolution (1.5 nm). Figure 4 compares the measured (black) and synthetic (gray) spectra for the copper sample, in 450 to 550 nm.

In the case of alumina targets, besides the aluminum and the oxygen, nitrogen and sodium in the synthetic spectra were also considered.

The experiments with beach sand were performed in order to examine the separation potentiality of our experimental setup for very complex targets. Ordinary beach sand was heat dried, pressed and sintered with the purpose of getting compact samples, which have a very complex composition and are inhomogeneous, i.e., the spectrum depends on the position the laser strikes the sample surface. It was not possible to build a synthetic spectrum because of the complexity and lack of information about the sample composition. We focused our attention to some peaks that are repetitive and very distinct from the background, by comparing their resonance wavelength with the NIST database. Several of the more intense observed lines were due to sodium and silicon, as shown in Fig. 5.

With regards to Mo samples, a Jobyn-Yvon spectrometer model TRIAX 550, with a 0.025 nm resolution (at 546 nm), was also used and plasma temperature was measured by means of the Boltzmann plot method (Amoruso *et al.*, 1999). The plasma temperature was about 0.9 eV, in agreement with results found in the literature for spectroscopic measurements (Noll, 2012;
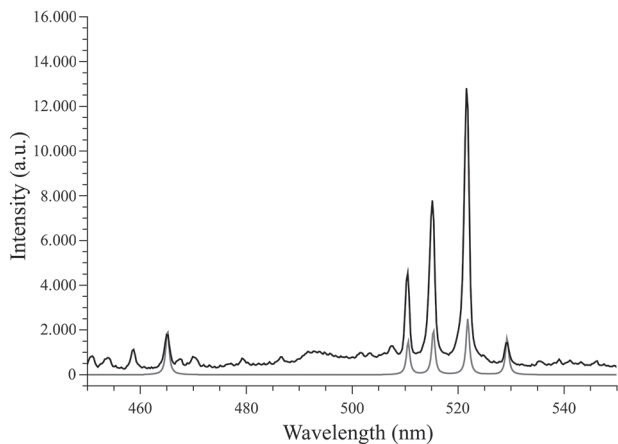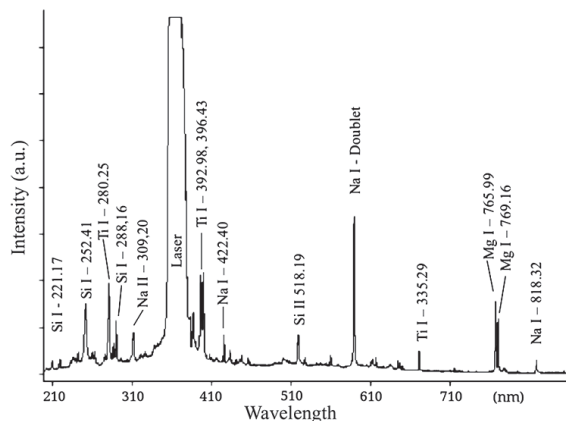

Figure 5. A typical sand LIBS spectrum. The saturated peak around 355 nm is due to the scattering of the laser beam.

Capitelli *et al.*, 2004), but in contrast with the results obtained in this work with Langmuir probe for other metallic samples.

ANALYSIS

In order to establish the magnitudes this work refers to, let us consider the experiments performed with tungsten targets and the CuHBr laser. The tungsten properties are: $a_A = 0.493$ for $\lambda = 511$ nm; $K = 1.74$ W/(cm ºC), $\kappa = 0.7$ cm²/s , atomic mass $M_W = 183.84$ amu, $c_E = 0.133$ J/(g ºC), $L_V = 4.48$ kJ/g, and $\rho_W = 19.3$ g/cm³. The laser parameters are provided in Table 1. With these, $T(0) \approx 100.000$ K. This temperature is much higher than the tungsten boiling point of 5,930 K (Lide, 1996), and before the surface had achieved this temperature level, a fraction of the sample had been evaporated and ejected, starting the formation of the ablation plume. This evaluation was done without taking changes of the thermal parameters with temperature into consideration, and without considering the interaction of the laser beam with the ejected plume. However, the value is in the same order of magnitude as the translational temperature measured, both with the PVDF sensor and the electrostatic probe. It means that the laser pulse energy is in some way delivered to the ejected plume.

Using Eq. 3, the mass that is removed in one single pulse is estimated in $m_E = 1.0 \times 10^{-7}$ g, which implies that, taking the laser repetition rate of 16 kHz, the ejected mass rate is about 5 g/h. This evaluation requires some care, and some fraction of the removed material expands as clusters and/or droplets. The following calculations assume that all the removed material is made of atoms (neutral or ionized). Thus, the obtained figures must be faced as limit values, which are useful only to provide orders of magnitudes for the analyzed parameters.

Figure 4. Comparison between measured (black line) and synthetic (gray line) spectra for copper samples.

If one takes an intermediate value for the expansion velocity (drift velocity) of $v_D = 5 \times 10^3$ m/s, at the end of the laser pulse the plume will expand a distance given by $L_E = v_D \tau \approx 175$ µm. The particle density (number of particles per unity of volume) at the end of the laser pulse can estimate if it is assumed that all evaporated material had been expanded to a volume given by a hemisphere with radius L_E as in Eq. 5:

$$n = \frac{m_E}{m_w} \frac{1}{2/3\pi L_E^3} \approx 2.9 \times 10^{19} \, cm^{-3}. \tag{5}$$

The mean free path is given by Eq. 6:

$$L_p = \frac{1}{n\sigma_c} \approx 560 nm, \tag{6}$$

where:

σ_C: the collisional cross section was estimated taking the tungsten atomic radius (1,41 Å) and thus $\sigma_C \approx 6.2$ barn.

Time between two successive collisions is given by Eq. 7:

$$\tau_C = \frac{L_p}{v_T} \approx 166 \text{ps} \tag{7},$$

where:

v_T: is the thermal velocity, calculated by taking the temperature of 100.000 K previously estimated.

Or rather, during a time period equivalent to the laser pulse duration, more than 200 collisions between particles happen in the plume. Kools *et al.* (1992), using Monte Carlo calculations, showed that only about four collisions are necessary for thermalization in the expanding plume. Thus, it is reasonable to consider that the plume expands similarly to a gas in equilibrium at high temperature and pressure, confined to a small volume, which is suddenly released to expand into vacuum.

The particle density decreases as the plume expands and, after some distance, the plume is not collisional anymore. To estimate this distance, it is considered that the particle density decays with the distance from the target surface according to Eq. 8,

$$n(z) = n(L_E)\left(\frac{L_E}{z}\right)^3 \tag{8}$$

and that the plume stops being collisional when the mean free path is in the same order of magnitude as the plume size L_p, thus substituting Eq. 8 into 6, one has Eq. 9:

$$L_{NC} = \sqrt{n(L_E)\sigma_C L_E^3} = 3.1 mm. \tag{9}$$

If one considers a 5 km/s expanding velocity, the time to expand until L_{NC} is in the order of 600 ns.

Therefore, for the experimental conditions presented in this work, after an expansion of about 3 mm, the plume is not collisional anymore and the interaction between particles from this point on is essentially electrostatic. Basically, two kinds of behavior are expected, for low densities the charged particles behave like free particles and for high densities they have a collective (plasma) behavior. The figure of merit that allows identifying the particles' behavior is the Debye Length L_{Db}, given by Eq. 10:

$$L_{Db} = \left(\frac{\varepsilon_0 k_B T_e}{q^2 N_e}\right)^{1/2}. \tag{10}$$

Taking the electron densities and temperatures from Table 3, the Debye length ranges from 0.5 to 2.6 mm in the present experimental conditions. Therefore, the plume typical dimensions are in the same order of magnitude as the Debye length and the particles' behavior is in the transition between the individual particles and plasma behavior regimes. It suggests that the charged particles (ions mainly) can be separated by the application of an electric field between electrodes apart from distances in the range of few millimeters and that the remaining plume fraction will be made of single atoms.

The same calculation was repeated for copper and aluminum, and the results, together with the values for tungsten, are presented in Table 4. The figures are very close and the same comments made for tungsten are also applicable for copper and aluminum.

Table 4. Estimated plume parameters for tungsten, copper, and aluminum, using the same calculation procedure described in "Analysis". The material constants were taken from Lide (1996), laser parameters from the CVL laser in Table 1 and plasma parameters from Table 3.

Parameters	Tungsten	Copper	Aluminum
Temperature at the surface (K)*	1.0×10^5	1.0×10^4	1.4×10^4
Removed mass per pulse (kg/pulse)	1.0×10^{-10}	1.6×10^{-11}	6.7×10^{-12}
Atom density (m⁻³)*	2.9×10^{25}	1.3×10^{25}	1.3×10^{25}
Mean free path (m)	5.6×10^{-7}	1.5×10^{-6}	1.2×10^{-6}
L_{NC} (m)	3.1×10^{-3}	1.9×10^{-6}	2.1×10^{-6}
Debye length (m)	5.0×10^{-4}	8.0×10^{-4}	1.8×10^{-3}

* at the end of the laser pulse.

CONCLUSIONS

In this work, several materials were evaluated in different experiments of laser ablation, using low energy (~ mJ per pulse), high repetition rate (~ tens of kHz) lasers in the visible and in the near ultraviolet, with pulse width in the range of tens of nanoseconds. The ablation experiments were in the thermal regime, with energy density in the range of tens of J/cm^2 and intensities of about 10^9 W/cm^2. The set of results for these experimental conditions leads to the following conclusions:

- a significant fraction of the plume generated by laser ablation is made of single atoms (neutral or ionized), even if complex targets are used;
- the ions and neutral atoms density are in the same order of magnitude;
- for distances greater than few millimeters, the plume is no longer collisional;
- at distances larger than 10 cm from the target, the Debye length is such that the charged fraction of the plume can be separated by the application of electromagnetic fields;
- ablation rates of about 5 g/h are possible.

In short, it is possible, using laser ablation, to generate an atomic beam adequate for AVLIS purpose. This is possible even for very complex targets, such as ores. The main limitation is the small amount of material that is removed, limiting the method for the separation of small amounts of material. This is a severe limitation for the separation of materials that are needed in large amounts, such as uranium, however it is adequate for the separation of materials used in photonics or in magneto-optic sensors, which require small amounts of isotopes.

REFERENCES

Amoruso, S. *et al.*, 1999, "Characterization of laser-ablation plasmas", Journal of Physics B: Atomic, Molecular and Optical Physics, Vol. 32, No. 14, pp. R131-R172. doi:10.1088/0953-4075/32/14/201

Beams, J.W. and Haynes, F.B., 1936, "The Separation of Isotopes by Centrifuging", Physical Review, Vol. 50, pp. 491-492. doi: 10.1103/PhysRev.50.491

Becker, E.W. *et al.*, 1967, "Separation of the Isotopes of Uranium by the Separation Nozzle Process", Angewandte Chemie International – Edition in English, Vol. 6, No. 6, pp 507-518. doi:10.1002/anie.196705071

Bennet, G.L., 2006, "Space Nuclear Power: Opening the Final Frontier", 4th International Energy Convertion Engineering Conference and Exhibit (IECEC), San Diego, California, USA, AIAA, pp. 2006-4191.

Born, M. and Wolf, E., 2002, "Principles of Optics: Electromagnetic Theory of Propagation: Interference and Diffraction of Light", 7th ed., Cambridge University Press, 952p.

Calusaru, A. and Murgulescu, S., 1976, "Chemical and Ion Exchange Unit for a Cascade of Uranium Isotope Separation", Naturwissenschaften, Vol. 63, No. 12, pp. 578-579. doi:10.1007/BF00622798

Capitelli, M. *et al.*, 2004, "Laser-induced plasma expansion: theoretical and experimental aspects", Spectrochimica Acta: Part B, Vol. 59, No. 3, pp. 271-289. doi:10.1016/j.sab.2003.12.017

Chung, P.M., 1975, "Electric probes in stationary and flowing plasmas: theory and applications", Springer-Verlag, New York, 150p.

Del Bosco, E. *et al.*, 1987, "Isotopic enrichment in a plasma centrifuge", Applied Physics Letters, Vol. 50, No. 24, pp. 1716. doi:10.1063/1.97725

Dolgolenko, D.A. and Muromkin, Y.A., 2009, "Plasma isotope separation based on ion cyclotron resonance", Physics Uspekhi, Vol. 52, No. 4, pp. 345-357. doi:10.3367/UFNe.0179.200904c.0369

Duley, W.W., 1976, "CO$_2$ Lasers: Effects and Applications", Academic Press, New York, 427p.

Flicker, H. *et al.*, 1964, "Construction of a promethium-147 atomic battery", IEEE Transactions on Electron Devices, Vol. 11, No. 1, pp. 2-8. doi:10.1109/T-ED.1964.15271

Furry, W.H. *et al.*, 1939, "On the theory of isotope separation by thermal diffusion", Physical Review, Vol. 55, No. 11, pp. 1083-1095. doi:10.1103/PhysRev.55.1083

Gião, M.A.P. *et al.*, 2004, "PVDF sensor in laser ablation experiments", Review of Scientific Instruments, Vol. 75, No 12, pp. 5213-5215. doi:10.1063/1.1819556

Itoh, N. *et al.*, 1999, "Small optical magnetic-field sensor that uses rare-earth iron garnet films based on the Faraday effect", Applied Optics, Vol. 38, No. 10, pp. 2047-2052. doi:10.1364/AO.38.002047

Jensen, R.J. *et al.*, 1982, "Separating isotopes with lasers", Los Alamos Science, Vol. 3, No. 1, pp. 02-33.

Kamada, O. *et al.*, 2009, "Mixed rare earth iron garnet (TbY) IG for magnetic field sensors", Journal of Applied Physics, Vol. 61, No. 8, pp. 3268-3270. doi:10.1063/1.338877

Kato, D. and Lamont, R.G., 1977, "Isotopic chemical vapor deposition of fused silica and high-silica-content glasses for the production of low-loss optical waveguides", Applied Optics, Vol. 16, No. 6, pp. 1453-1454. doi:10.1364/AO.16.001453

Kholpanov, L.P. *et al.*, 1997, "Multicomponent isotope separating cascade with losses", Chemical Engineering and Processing: Process and Intensification, Vol. 36, No. 3, pp. 189-193. doi:10.1016/S0255-2701(96)04187-6

Kim, D.W. *et al.*, 2001, "Separation of magnesium isotopes by ion exchange chromatography", Journal of Industrial and Engineering Chemistry, Vol. 7, No. 3, pp. 173-177.

Kools, J.C.S. *et al.*, 1992, "Gas flow dynamics in laser ablation deposition", Journal of Applied Physics, Vol. 71, No. 9, pp. 4547-4556. doi:10.1063/1.350772

Koopman, D.W., 1971, "Langmuir probe and microwave measurements of the properties of streaming plasmas generated by focused laser pulses", The Physics of Fluids, Vol. 14, No. 8, pp. 1707-1716. doi:10.1063/1.1693667

Lide, D.R., 1996, "CRC Handbook of Chemistry and Physics", 76th ed., CRC Press, Boca Raton, USA, 2650p.

Louvet, P., 1995, "Device for isotope separation by ion cyclotron resonance", Patent US005422481A.

Mack, E. and Arroe, H., 1956, "Isotope shift in atomic spectra", Annual Review of Nuclear Science, Vol. 6, pp. 117-128. doi:10.1146/annurev.ns.06.120156.001001

Martynenko, Y.V., 2009, "Electromagnetic isotope separation method and its heritage", Physics-Uspekhi, Vol. 52, No. 12, pp. 1266-1272. doi:10.3367/UFNe.0179.200912n.1354

Naylor, R.W. and Backer, P.O., 1955, "Enrichment calculations in gaseous diffusion: Large separation factor", AIChE Journal, Vol. 1, pp. 95-99. doi:10.1002/aic.690010114

NIST 2012, "NIST Atomic Spectra Database Lines Form", Retrieved in Mach 08, 2012, from http://physics.nist.gov/PhysRefData/ASD/lines_form.html.

Noll, R., 2012, "Laser-induced breakdown spectroscopy", Springer-Verlag, Heidelberg, 543p. doi:10.1007/978-3-642-20668-9

Paisner, J.A., 1988, "Atomic Vapor Laser Isotope Separation", Applied Physics B: Lasers and Optics, Vol. 46, No. 3, pp. 253-260. doi:10.1007/BF00692883

Prasad, R.R. and Krishnan, M., 1987, "Theoretical and experimental study of rotation in a vacuum arc centrifuge", Journal of Applied Physics, Vol. 61, No. 1, pp. 113-119. doi:10.1063/1.338976

Riley Jr., J.E., 1987, "The effects of lithium isotopic anomalies on lithium niobate", Ferroelectrics, Vol. 75, No. 1, pp. 59-62. doi:10.1080/00150198708008209

Rutherford, W.M., 1986, "Separation of Zinc Isotopes by Liquid-Phase Thermal Diffusion", Industrial & References Engineering Chemistry Process Design and Development, Vol. 25, No. 4, pp. 855-858. doi:10.1021/i200035a003

Schiller, S. *et al.*, 1983, "Electron Beam Technology", John Wiley & Son, New York, Chichester, Brisbane, Toronto, Singapore, 508p.

Schwab, C. *et al.*, 1998, "Laser techniques applied to isotope separation of uranium", Progress in Nuclear Energy, Vol. 33, No. 1/2, pp. 217-264. doi:10.1016/S0149-1970(97)00100-5